University of Texas at El Paso

ScholarWorks@UTEP

2022-12-01

The Qualification Of Sealability And Creep Relaxation Of Additively Manufactured Zytel Gaskets For Pem Fuel Cells

Robert Lazarin
University of Texas at El Paso

Follow this and additional works at: https://scholarworks.utep.edu/open_etd

Part of the Mechanical Engineering Commons, Mechanics of Materials Commons, and the Oil, Gas, and Energy Commons

THE QUALIFICATION OF SEALABILITY AND CREEP RELAXATION OF

ADDITIVELY MANUFACTURED ZYTEL GASKETS

FOR PEM FUEL CELLS

ROBERT ANTHONY LAZARIN

Master's Program in Mechanical Engineering

APPROVED:

_____

Yirong Lin, Ph.D., Chair

_____

Calvin M. Stewart, Ph.D.

_____

David Espalin, Ph.D.

_____

Tommy Rockward, M.S

_____

Stephen Crites, Ph.D.
Dean of the Graduate School

DEDICATION

To God and my family.

THE QUALIFICATION OF SEALABILITY AND CREEP RELAXATION OF ADDITIVELY

MANUFACTURED ZYTEL GASKETS FOR PEM FUEL CELLS

by

ROBERT ANTHONY LAZARIN, B.S.

THESIS

Presented to the Faculty of the Graduate School of

The University of Texas at El Paso

in Partial Fulfillment

of the Requirements

for the Degree of

MASTER OF SCIENCE

Department of Aerospace and Mechanical Engineering

THE UNIVERSITY OF TEXAS AT EL PASO

DECEMBER 2022

ACKNOWLEDGMENTS

ABSTRACT

The purpose of this thesis is to study the feasibility of low-cost additive manufacturing of gaskets for proton exchange membrane fuel cells exposed to extreme temperature conditions ranging from -55°C to 100°C. With the growing popularity and decreasing costs of additive manufacturing technologies, specifically Material Extrusion (ME), research is being conducted to determine the feasibility of ME components. Thermally cycled PEMFCs may exhibit accelerated gasket deterioration, therefore, the mechanical stability of material extruded gaskets following a harsh thermal cycle must be assessed.

The feasibility of the material extruded gaskets will be proven by manufacturing optimization and mechanical testing. The target material for this study is Zytel by DuPont Chemical. The mechanical stability will be assessed via sealability and creep relaxation testing according to ASTM F37B and ASTM F38B respectively. Because the capabilities to conduct sealability testing at temperature were not available, each specimen was thermally soaked and allowed to return to room temperature prior to testing.

As a result of sealability experiments, the 100°C-soaked specimens resulted in lower leak rates with a higher precision when compared to specimens soaked at -55°C and 22°C at across all compressive loads. It was observed from results from creep relaxation testing that there is thermal contraction and expansion occurring at 55°C and 100°C respectively, which can be observed by the resultant graphs. The recoverability of thermally cycled specimens are better than those that just experience a high temperature hold. After the seven-day thermal cycle, the samples stabilized and maintained their structure.

TABLE OF CONTENTS

LIST OF FIGURES

LIST OF TABLES

NOMENCLATURE

ABS	Acrylonitrile Butadiene Styrene
AM	Additive Manufacturing
ASTM	American Society for Testing and Materials
ATR-FTIR	Attenuated Total Reflection Fourier Transform Infrared Spectroscopy
BPP	Bipolar Plates
CO_2	Carbon Dioxide
CAD	Computer Aided Design
°	Degree
°C	Degree Celsius
DMA	Dynamic Mechanical Analysis
EDS	Energy Dispersive X-ray Spectroscopy
EPDM	Ethylene Propylene Diene Monomer
FSR	Fluorosilicone Rubber
GDL	Gas Diffusion Layer
GISAXS	Gracing Incidence Small Angle X-ray Scattering
hr	Hour
HF	Hydrofluoric Acid
H^+	Hydrogen Ion
ME	Material Extrusion
MPa	Megapascal
MEA	Membrane Electrode Assembly

mL	Miliiters
mm	Millimeters
min	Minutes
O_2	Oxygen
PLA	Polylactic Acid
PTFE	Polytetrafluoroethylene
PSI	Pound Per Square Inch
PEM	Proton Exchange Membrane
PEMFC	Proton Exchange Membrane Fuel Cell
SEM	Scanning Electron Microscope
STL	Stereolithography
H_2SO_4	Sulfuric Acid
3D	Three Dimensional
XCT	X-ray Computed Tomography
XRD	X-ray Diffraction

1 INTRODUCTION

1.1 MOTIVATION

In a global effort to reduce the total carbon emissions, there has been a massive rise in popularity of the hydrogen economy. It is believed that hydrogen will play a crucial role in the decarbonization of the large contributors of CO_2 such as energy generation and transportation.
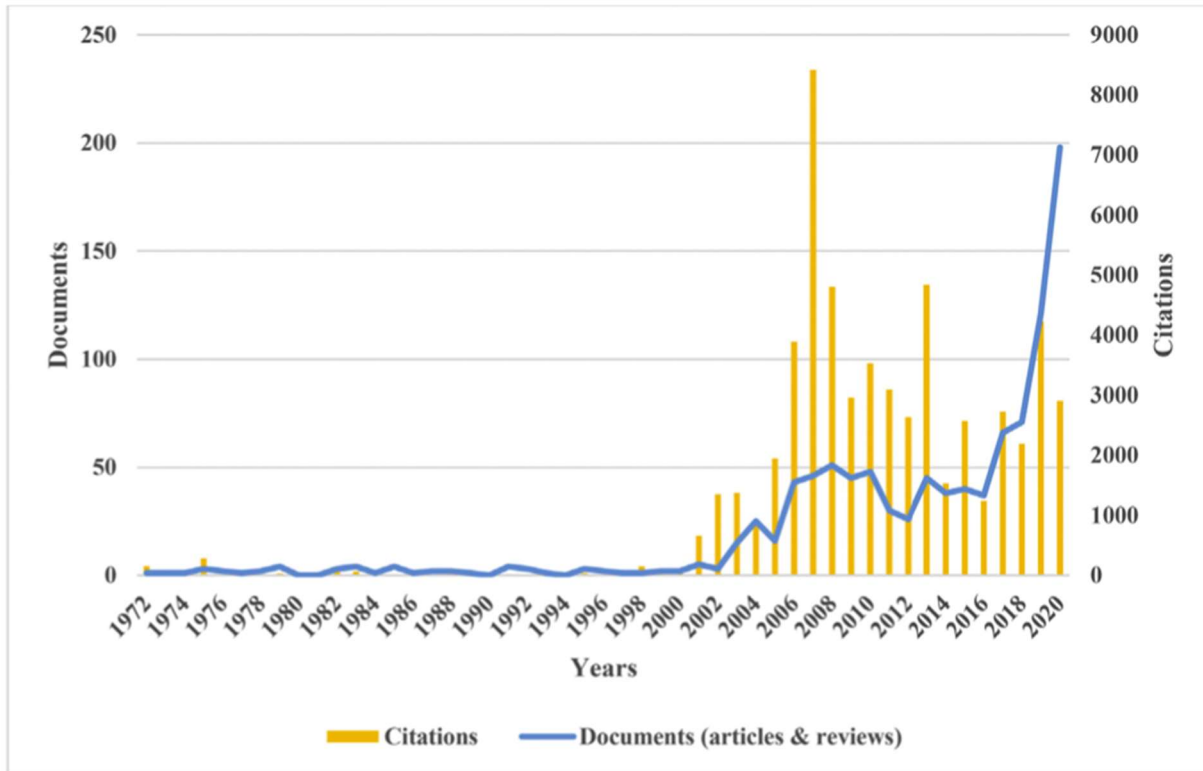
Figure 1: Documents Published and Citations received on Hydrogen Economy Over the Years (Data Until August 2021) [1]

The popularity spike of hydrogen economy publications is visualized in Figure 1. Rather than the increase of work being conducted having a unilateral focus such as the storage or production of hydrogen, the publications are focused on the entirety of the hydrogen economy [1-2].
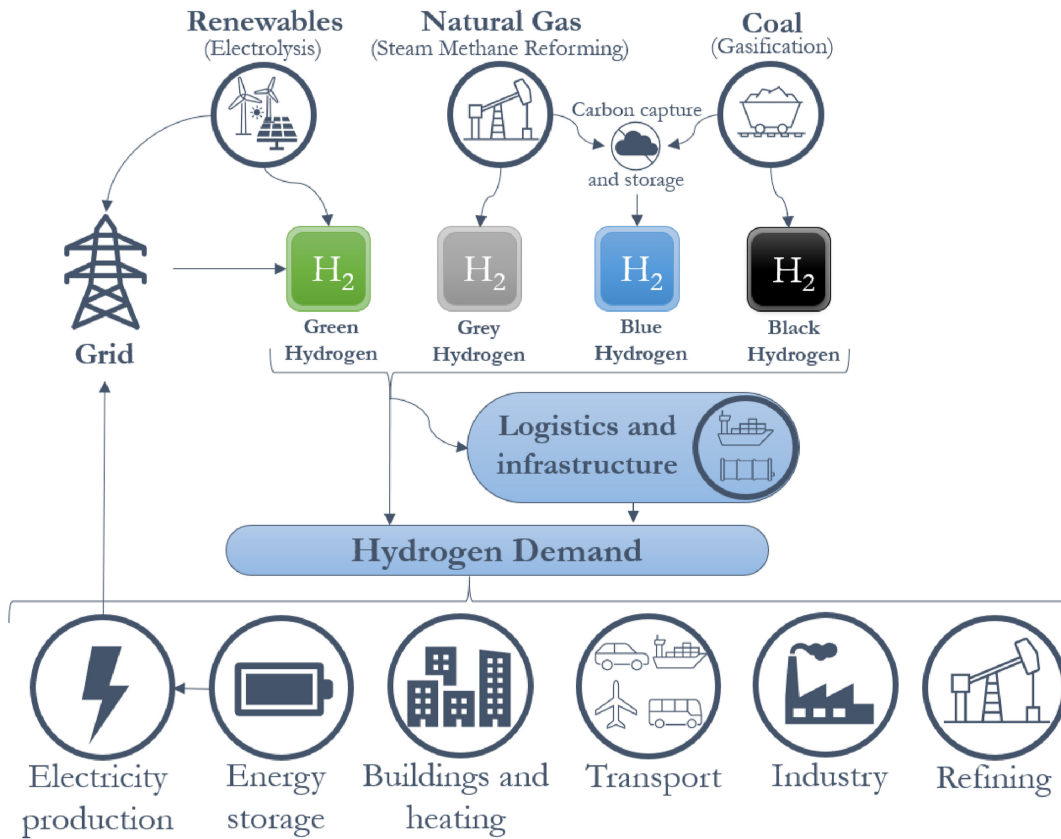
Figure 2: Simplified Schematic of the Hydrogen Economy [3]

A simplified schematic of the hydrogen economy cycle is shown in Figure 2. The three major areas of focus are the production, supply/distribution, and end use of hydrogen. There are currently four distinct classifications of hydrogen, grey, black (or brown), green, and blue, each with their own different production processes. The current hydrogen production methods are highly carbon and fossil fuel based, roughly 96%, and yield black and grey hydrogen. Grey hydrogen is produced via a process known as steam methane reforming of natural gas [4]. Black

hydrogen is produced through a process known as gasification from coal [5]. The decarbonization on a global scale requires the transition to the production of both blue and green hydrogen, both cleaner alternatives to the current methods. Blue hydrogen still requires the use of steam methane reforming but adds the utilization of carbon capture to make the process greener. Green hydrogen is produced via electrolysis powered by a form of renewable energy sources such as solar or wind [6-8].
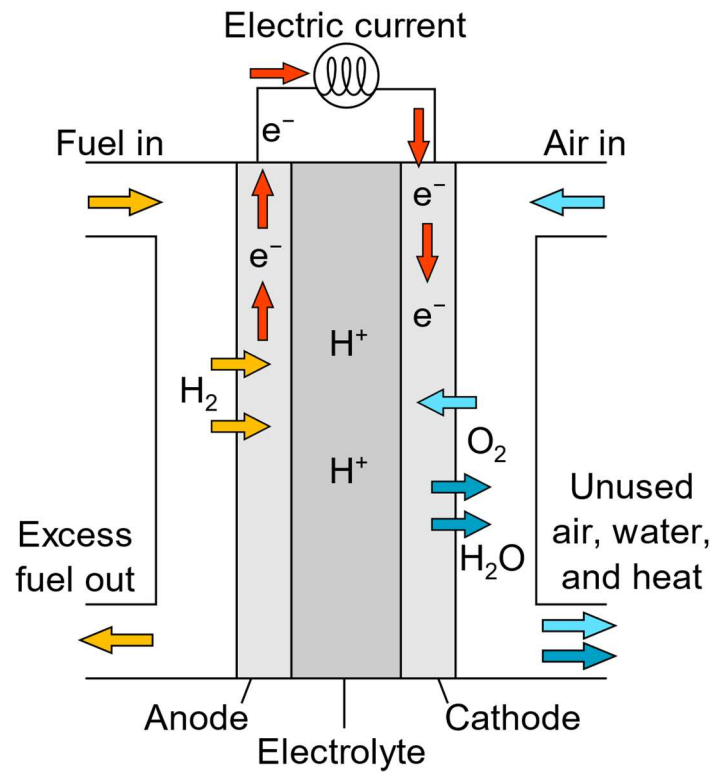
Figure 3: PEM Fuel Cell Electrochemical Process

In order to maintain the zero-emission mission, proton exchange membrane fuel cells (PEMFC's) are a popular solution as they produce electricity with heat and water as the sole waste products of the chemical reaction [9]. Proton exchange membrane fuel cells belong to the family of electrochemical fuel cells which all function on the basis of converting chemical energy to

electrical energy via redox reactions [10]. The hydrogen gas is oxidized at the anode electrode and the electrons that are stripped from the atom are conducted through an external circuit generating electricity. The H^+ ions are passed through the membrane electrode assembly (MEA) to the cathode side where the H^+, $\frac{1}{2}$ O_2, and oxidized electrons are reduced and form water and heat as the only byproducts making a PEMFC a green energy source (Figure 3). This process must be sealed with gaskets to prevent leaking of the hydrogen fuel outside of the cell as well as crossover leakage of hydrogen and oxygen gases across the MEA which results in decreasing efficiency eventually leading to catastrophic failure of the cell and/or stack [11].

The advancement of additive manufacturing (AM) technologies has enabled far more complex structures to be fabricated than ever before. Additive manufacturing has been applied in various sectors such as aerospace, automotive, and even the 3D printing of functional organic tissue [12-14]. The rapidly growing demand for hydrogen-based energy production has opened work on producing highly efficient and durable proton-exchange membrane fuel cells. To cut down on development costs, AM, specifically Material Extrusion (ME), is seen as a low-cost solution to rapid prototyping and material selection. The focus of this study is to evaluate a low-cost additive manufacturing technology for its feasibility as a rapid prototyping technique for PEMFC gaskets.

1.2 LITERATURE REVIEW
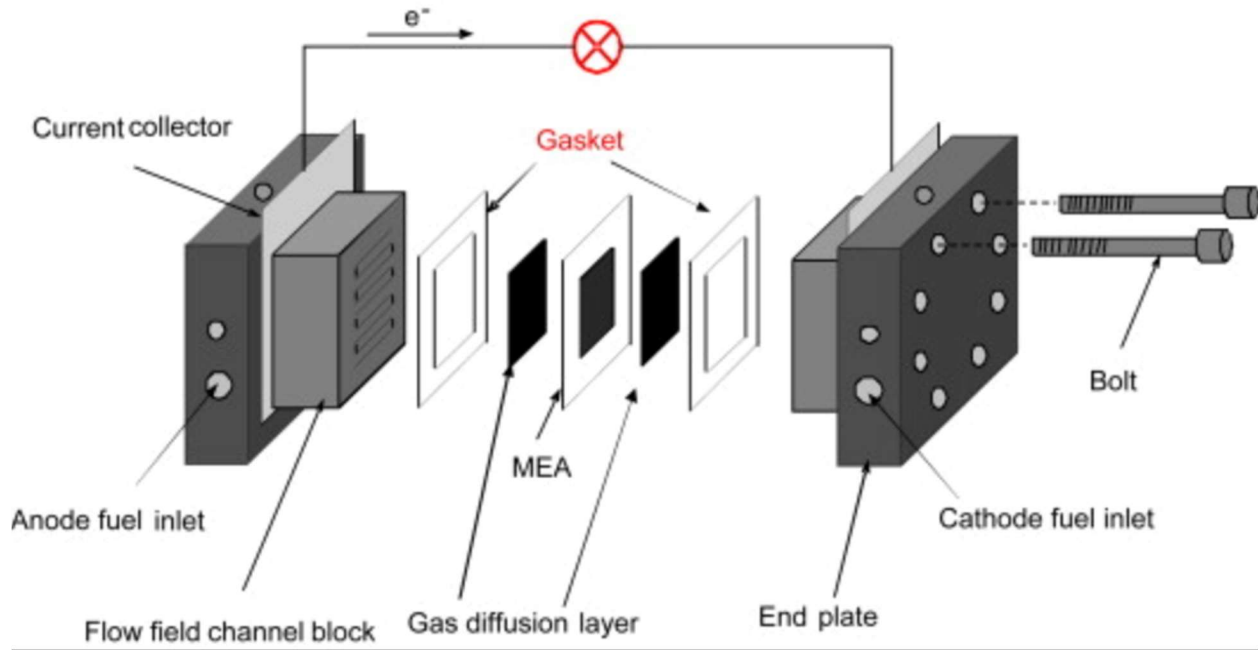
Figure 4: Exploded View of Various PEMFC Components

A proton exchange membrane fuel cell is comprised of multiple important components which are showcased in Figure 4. The individual components that make up a singular cell in a stack are the end plates, flow field channel plates or bipolar plates (BPP), gas diffusion layers (GDL), membrane electrode assembly (MEA), two electrodes (anode and cathode) and gaskets. Individual fuel cells can be stacked in series with one another to generate more electricity, which in total is the summation of the individual cell outputs. The gaskets and bipolar plates are referred to as the PEMFC hardware components which together serve the purpose of fluid distribution and management (reactant gas and water), current collection, and gas containment within the system [15].

As the fuel cell is carefully assembled, the gaskets are normally positioned in between the bipolar plates to generate a seal that encases the entire chemical reaction. The key responsibilities

that gaskets serve are to prevent both external and cross-over leakage of reactant gases as well as maintain electrical insulation of the fuel cell components. The gasket while in service is exposed to mechanical loading via compression, humidity, hydrogen, and a liquid acidic solution. This is why the stability of the gasket is paramount the performance, durability, and safety of the fuel cell [16].

Mechanical stability is defined as compression set and creep relaxation in gaskets. Compression is used to seal individual fuel cells as well as to hold a fuel cell stack together. Because the target temperature of this study ranges from -55°C to 100°C, compression tests must also be conducted at those temperatures to determine the stability of the material [17]. Elastomeric materials for these gaskets tend to have a higher compressibility and higher recoverability percentages when compared to thermoplastic materials which can lead to severe deformation in larger, pressurized fuel cell stacks. This deformation results in overall failure in the fuel cells as they can experience crossover leakage and gas flow blockages [18].

The thermal and chemical stability of gasketing materials is crucial to maintaining the integrity and longevity of the fuel cell. Traditional PEM fuel cell operation occurs between 70°C and 90°C where the gasket is stable due to the cell not being subjected to massive temperature swings [16]. The target temperatures of this study ranging from -55°C to 100°C will require the testing of the gasket materials at those temperatures to determine thermal stability. If the gasket material experiences severe thermal expansion and/or contraction of a gasket can lead to a loss in seal integrity that results in crossover leakage and catastrophic failure of the fuel cell. It has been shown that annealing polymers results in the resolution of residual stresses and stabilizes the crystal structure of the polymer which then stabilizes the material the material at annealing temperature [19].

The gasket must exhibit superior chemical resistance. The internal components of the PEM fuel cell will be exposed to humidity, pure hydrogen gas, standing water, and sulfuric acid (from the MEA assembly) [9]. Humidity combined with the compressive load can lead to the formation of decomposition products that lead to the poisoning of the catalysts [20]. Like accelerated creep testing, accelerated chemical degradation testing can be conducted and coupled with dynamic mechanical analysis (DMA), can accurately be used to track, and estimate gasket lifetime [21]. Scanning Electron Microscopy (SEM) and Energy Dispersive X-ray Spectroscopy (EDS) can be utilized to track the surface degradation of aged gaskets [20].
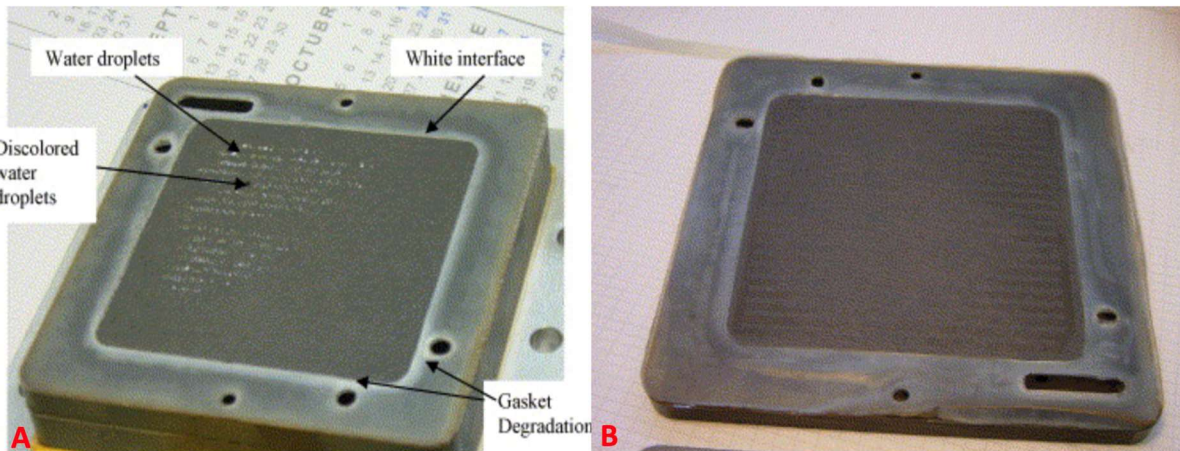
Figure 5: Comparison of (A) Failed Gasket and (B) Undegraded Gasket [11]

The failure mechanisms of proton exchange fuel cell stacks is highly investigated. Husar et al. examined the failure mode for a fuel cell stack comprised of seven individual fuel cells. It was concluded that the stack failed because of a crossover leak on the cathode side of a single fuel cell. The crossover leak developed due to the gasket of the cell degrading with fuel cell operation which can be seen in Figure 5A. The degradation of the gasket can be identified by the severe discoloration of the edges of the gasket near the GDL. An undegraded gasket from the same fuel

cell stack can be seen in Figure 5B. The undegraded gasket does not show major discoloration similar to that seen on the failed gasket. The degradation is suspected to be initiated with loosening of the stack caused by thermal cycling of the cell stack. The leak continued to grow leading to small combustions occurring due to pure oxygen and hydrogen mixing. Eventually, the leak grew so large that the crossover leakage of oxygen into the anode side of the fuel cell leading to a dramatic increase in temperature and stack failure. It was observed that the heat was so intense that the gasket melted and fused to the MEA at the anode inlet port [11].

As popular as PEMFC research is, the work conducted investigating gaskets is very limited. The majority of work being done on gaskets includes elastomeric materials and a single thermoplastic. Elastomeric materials offer a great sealing with minimal load applied but are susceptible to deformation which can lead to bipolar plate blockages. Thermoplastics offer superior mechanical stability under compression but requires more load to achieve the same sealability as an elastomer.

Wei Lin et al. gave segway into materials that are currently being considered for gasketing PEM Fuel Cells. It allowed for early acknowledgement of flourosilicone rubber and ethylene-propylene-diene monomer (EPDM) as promising candidates for our solution. It also gave information on how these materials behaved in a simulated PEM fuel cell environment. The solution in the environment is like that of an actual PEM fuel cell which consisted of 48% HF and 98% H_2SO_4 dissolved in reagent grade water [21].

Tan et al. gave insight to how EPDM behaves in a PEMFC environment both chemical and mechanical. The solution used to simulate a PEMFC environment is the same used in Wei Lin. The test was completed using different EPDM specimens aged using the same solution but aged at 2 different temperatures which were 60°C and 80°C for 1-35 weeks. The specimens were

then removed from the solution and analyzed using attenuated total reflection Fourier transform infrared (ATR-FTIR) spectroscopy, atomic absorption spectrometry, micro-indentation test, and dynamic mechanical analysis (DMA). After the micro-indentation test and DMA, it was concluded that after 35 weeks of testing, surface hardening did not occur. It was also stated that the mechanical properties did not change significantly after the 35-week aging and heating cycle [22].

Tan et al. conducted the same study but on Silicone S. The micro-indentation tests concluded that after 46 weeks that Silicone S surface hardening did occur in Silicone S and that the elastic modulus increased through aging. DMA showed that the mechanical properties like storage modulus, loss modulus, and glass transition temperature did not change after the 46 weeks aging process [23].

Shen et al. investigated the effect of multilayered EPDM gaskets (like sandwich gaskets) The multilayered vulcanizate consists of alternating layers of soft and hard layers. The multilayered vulcanizates offer a lower tensile strength and compression set when compared to blended vulcanizates but had a higher hardness. The higher hardness and lower compression ultimately result in a higher sealing force, better stability, better sealing capacity, and ultimately a longer working life. This behavior is similar to what thermoplastic materials such as PTFE offer [24].

Determining the desired gasket requirements is difficult as there are little to know specifications determining maximum allowable leak rates or stress relaxation. The current Department of Energy (DOE) technical targets include targets for membrane electrode assemblies, bipolar plates, overall fuel cell efficiency, and catalysts but fail to mention specifics on gasketing materials [25]. Scientists at Los Alamos National Laboratory determined the maximum allowable

leak rate for hydrogen fuel cells to be $1.0 \times 10^{-4} \ cm^3/s$ [26]. This value converts to $6.0 \times 10^{-3} \ mL/min$, the unit used in this study to define leak rate.

1.3   RESEARCH OBJECTIVES

The objective of this study is to qualify the sealability and creep relaxation behavior of the additively manufactured candidate material, Zytel, for service in proton exchange fuel cells. Additive manufacturing via material extrusion allows for the low cost rapid prototyping the during optimization iteration phase of designing new features. This thesis work is considered valid upon the completion of these three objectives.

1.3.1   Research Objective #1 (RO1): Initial Materials Screening

The goal of this objective is to conduct extensive literature to identify potential gasket materials that are functional for PEM fuel cell applications. The materials must satisfy the temperature range of -55°C to 100°C while also remaining mechanically stable and chemically resistant.

1.3.2   Research Objective #2 (RO2): Optimizing the Printing Parameters

The goal of this objective is to optimize the printing parameters of the candidate material. This will enable the gaskets to be fabricated ideally absent of any printing flaws for the testing for this study.

1.3.3   Research Objective #3 (RO3): Sealability and Creep Relaxation Qualification

The goal of this objective is to qualify the candidate material's sealability and creep relaxation behavior according to ASTM standards. The results of these experiments will qualify the candidate material mechanically stable and suitable for sealing in PEMFC's.

1.4   ORGANIZATION

The work in this thesis is organized as follows:

Chapter 2 explains the results of extensive literature review and the reasoning behind selecting the target material for this study. Chapter 3 describes the additive manufacturing process and it's optimization in order to result in near perfect gasket specimen. The optimized printing parameters and their importance is elaborated. Chapter 4 explains in detail the methodology of this study to qualify the gaskets sealability and creep relaxation behaviors. Chapter 5 presents the results of the gasket characterization which includes sealability, creep relaxation, x-ray diffraction analysis, and microscopy of the thermally soaked specimen. Chapters 6 and 7 contain the concluding remarks on the feasibility of additive manufacturing for PEMFC gasket and proposals for future work that is left to be conducted.

1.5 EQUIPMENT USED

Figure 6 - Creatbot F430 FFF 3D Printer

The Creatbot F430 3D printer utilized to fabricate the sample gaskets is shown in Figure 6. This dual extruder 3D printer is a high precision printer with a printing accuracy of .04mm. Its two direct drive Hotends can reach temperatures of up to 260°C for the left nozzle and 420°C for the right nozzle, and the bed can reach temperatures of up to 140°C. The lower temperature nozzle is used for materials such as nylon, ABS, and PLA, whereas the higher temperature nozzle is used for materials that are a bit more abrasive such as metal fused filament for fused filament fabrication. It is a fully enclosed printer which ensures a stable environment for any print, and its metal chassis makes this printer durable.

Figure 7: Tenney Test Chamber TJR-A-F4T

A Tenney environmental testing chamber is utilized for the thermal soaking of test specimen is seen in Figure 7. The model of the chamber is Tenney Test Chamber TJR-A-F4T with a 1.25 cubic foot test chamber. The test chamber is capable of temperatures as low as -75°C with a maximum of 200°C. The dimensions of the chamber, 16" x 11" x 11.75" (W x D x H), allows for all specimen in an isotherm series to be soaked simultaneously with a tolerance of +/-1°C. The flaw of this chamber is that it lacks any humidity control making the environment susceptible to humidity fluctuations which can possibly affect specimen.

Figure 8 - Keyence VHX-970F (a) microscope (b) lens

The microscope employed for this study is a Keyence VHX-970F digital microscope equipped with a 20x to 2000x lens is employed to evaluate the AM build quality is shown in Figure 8. This power is divided into two lenses, a low and high-power lens. The low-power lens ranges from 20x to 200x and the high-power lens offers a range from 200x to 2000x magnification. The VHX software that comes with the microscope allows for the user to snap high resolution images and video which can be used to obtain precise and accurate measurements of observed features and overall size. The software automatically generates tags such as the scaling of an image, magnification, time, and date. The microscope allows for multi angle observation while not sacrificing image quality which aids in the rapid qualification of the AM parts.
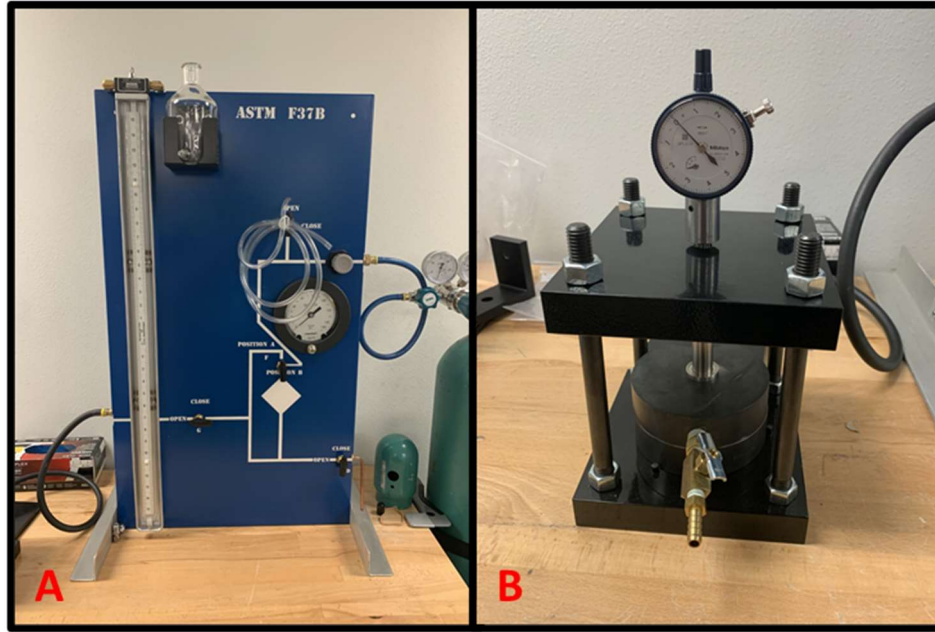
Figure 9: (A) ASTM F37 Test Panel (B) Cell Cage Assembly

An ASTM F37B test assembly from Metal Samples is employed to measure the gas sealability of gasket materials shown in Figure 9. The specimen for this standard is an annular one with an outer diameter of 44.20 to 44.32 mm (1.740 to 1.745 in.) and an inner diameter of 32.26 to 32.31 mm (1.270 to 1.272 in.). The gasket sits in between two metallic platens which is compressed by the turning of 4 nuts to the desired displacement, which is directly correlated to compressive load applied to the gasket, reading a dial indicator. The system is tested at a maximum internal pressure of 30 psi using dry nitrogen. The only leak point on the system is the interface between the gasket and platens. Leakage is determined by changes in the water level inside of the manometer. The total time it takes for the water level to change by a total of three tick marks (one tick mark is equal to one-tenth of an inch) is used to calculate the overall leak rate.

Figure 10: ASTM F38 Testing Assembly

An ASTM F38B test assembly from Metal Samples is employed to measure the creep relaxation behavior of the gasket materials is shown in Figure 10. The standard calls for annular test specimen have an outer diameter of 43.46 mm (1.715 in.) and an inner diameter of 15.621 mm (0.615 in.) with a thickness of 1.6 mm (0.625 in) +/- 0.127 mm (0.005 in). An individual test assembly is comprised of two platens, where the gasket sits in-between, a thoroughly calibrated bolt, washer, nut, and a dial indicator. The displacement recorded by the dial indicator directly correlates to the compressive load applied to the platens and gasket. The difference in the dial indicator's reading pre and post-test is used to determine the creep relaxation behavior of the material.

Figure 11: Bruker D8 Discover XRD

The Bruker D8 Discover was employed for x-ray diffraction analysis (XRD) to determine any changes in the crystallinity of the specimen, which would be indicative of thermal annealing having occurred. The Bruker D8 is capable of both diffraction and scatter analysis for all research applications. The D8 Discover is capable of qualitative and quantitative phase analysis, structure analysis, high resolution XRD, reflectometry, reciprocal space mapping, grace incidence diffraction, gracing incidence small angle X-ray scattering (GISAXS), stress and texture analysis, and micro-diffraction.

2 INITIAL MATERIALS SCREENING

2.1 INITIAL MATERIALS

Table 1: Summary of Mechanical Properties Important for Fuel Cell Gaskets

Material	Acronym	Type	Printable (Material Extrusion)	Tensile Strength (MPa)	Elongation (%)	Density (g/cm^3)	Water Absorption (%)	Low Temperature (°C)	High Temperature (°C)	Chemical Resistance	Compressibility
Nylon 66	Zytel	Thermoplastic	Yes	75	13	1.23	1.2	-40	120	Moderate	Poor
Polytetrafluoroethylene	PTFE	Thermoplastic	Maybe	24.9	318	2.17	<.01	-183	261	Good	Poor
Ethylene Propylene Diene Monomer	EPDM	Rubber	No	17	300	0.86	1	-50	150	Good	Good
Fluorosilicone Rubber	FSR	Rubber	No	8	>300	1.25	1.57	-60	220	Good	Good

After conducting a thorough literature review, four polymers were identified as potential candidate materials as gaskets in the PEMFC's in extreme temperature environments. The four identified polymers are ethylene propylene diene monomer (EPDM), fluorosilicone rubber (FSR), polytetrafluoroethylene (PTFE), and Zytel by Dupont. A table which describes the desired preliminary mechanical properties can be found in Table 1 and how the potential material candidates compare to one another [21, 27-32]. The table is color coded in order to aid in the distinction between a good property (highlighted in green), a moderate property (highlighted in orange), and a bad property (highlighted in red). The table contains basic information about the materials such as the tensile strengths and elongation percentages but also has key material properties such as the operating temperature ranges and the material's chemical resistance. The most important parameter on the material matrix is the materials ability to be manufactured via material extrusion, being that this is the selected process for manufacturing for this study. Chemical resistance/stability and water absorption were selected as important mechanical properties as the gasket will be in contact with reactant gasses and water as a result of the chemical reaction, it is integral to not chemically degrade to the acidic environment or become saturated with water to prevent the formation of ice internally at low temperatures. Temperature stability is key to a PEM fuel cell gasket that is expected to resist thermal degradation to maintain its strong seal through multiple thermal cycles and extended holds. Compressibility affects how easily a gasket can produce a seal. A thermoplastic like PTFE requires a greater compressive force to create a seal compared to an elastomer such as EPDM. A higher compressive force can result in a decrease in efficiency or damage to the gasket and other key hardware components such as the bipolar plates, membrane electrode assemblies (MEA's), or gas diffusion layers (GDL's). If the gasket fails in any of the mentioned areas during operation, there would be a high chance for loss

of property and damage to life depending on how severe the leak(s) were and if the reactant gases mixed together.

2.2 SUBJECT MATERIAL: ZYTEL

Figure 12: (A) Zytel Packaging and (B) Zytel Filament Spool in Printer

After reviewing the identified materials and their key mechanical properties, Zytel was selected as the target material due it's unique ability to safely and easily be fabricated via material extrusion, the chosen additive manufacturing method for this research. The specific name for the Zytel blend used for this study is Dupont Zytel 3D1000FL filament with a diameter of 1.75 mm as imaged in Figure 12 [33]. The filament is vacuum wrapped to prevent humidity and other airborne contaminants from affecting the filament during shipment and storage. The filament is white and very smooth in nature making it easier to install into the printer. The suggested nozzle temperature

for material extrusion printing is between 245 to 295°C with a bed temperature between 85 to 110°C [34]. Zytel is an extremely popular and widely used engineered thermoplastic that exhibits high stiffness and strength with outstanding heat, chemical, and hydrolysis resistance as listed in Table 2 [27, 33-35]. Zytel is currently employed in fuel cell stack systems as hoses and pipes in the air and thermal management systems, insulator plates water covers in the fuel cell, and as the hydrogen tank liner of the fuel processing system.[35]

Table 2: Factory Mechanical Properties of Zytel

Min. Operating Temperature °C (°F)	Max Operating Temperature °C (°F)	Ultimate Tensile Strength MPa (psi)	Durometer (Hardness)	Elongation (%)	Water Absorption (%)
-40°C	260°C (500°F)	40 (5802)	79M	15	7.6

3   ADDITIVE MANUFACTURING

3.1   MATERIAL EXTRUSION OPTIMIZATION

Every roll of filament, even if it is the same material, varies from each other. This can be due to factors such as the manufacturing processes, dye used, or how much moisture has been absorbed. Every time a new roll of filament is used, the previous parameters may not execute quality prints. A calibration process that quickly allows optimal parameters to be selected has been designed.

All tests were performed via material extrusion (otherwise known as fused deposition modeling). Material extrusion pushes filament through a heated nozzle and selectively deposits said material layer by layer [36]. A general starting place for speed is 40 mm/s, which the calibration tests were performed at. Most prints are done between 20 mm/s through 100 mm/s. The median speed was chosen. Time to print was reduced, compared to 20 mm/s, without sacrificing the quality. The website, *Thingiverse*, allows enthusiasts to upload files for others to use. There are many different types of tests uploaded that are used to improve print quality.

Temperature affects the overall print quality [37]. Commercial brought filament provides a predetermined temperature printing range and bed temperature. Temperature influences the quality of the prints. Therefore, the predetermined range is given to help find the optimal print temperature. The temperature range allows for the material to be extruded without clogging the nozzle, on the lower end, or liquefying the material, on the higher end. Once an acceptable range has been determined, the best temperature needs to be optimized. Determining the optimal temperature allows for the filament to give clean and precise prints.
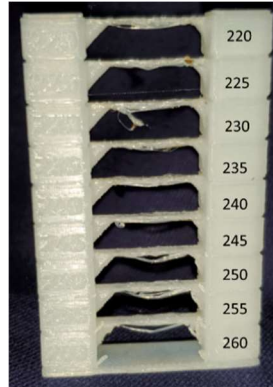
Figure 13: Temperature Tower

A temperature tower consists of two towers separated into sections, with a bridge connecting the corresponding section as illustrated in Figure 13. The bottom section is the highest allowable temperature and is decreased by 5 degrees Celsius for every section up the tower. After the tower is printed, it is visually inspected. Areas with the smoothest, least number of flaws, and least amount of stringing on the bridge is considered the optimal temperature [38].

Next, layer adhesion is considered. Poor layer adhesion leads to a poor mechanical structure [39]. Starting at the coldest temperature, try to pull apart the structure with hands or pliers. This gives a sense of what temperatures have a sound structure. If only a visually appealing print is needed, choose the print temperature solely based on the temperature tower. However, if only the strength needs to be considered, a temperature is chosen based off the layer adhesion. If both need to be taken into consideration, a temperature is selected in this range.

Retraction is when the extruder retracts a specified length of filament back into the nozzle. A common issue in material extrusion is stringing. Stringing is when small amounts of filament are left behind and forms strings or blobs; also known as oozing, whiskers, or hairy. The retraction feature prevents unwanted filament from leaking; therefore, stringing is eliminated.

Since the optimal temperature is set, a retraction test is performed to discover the correct retraction distance needed to eliminate this issue [40].

Figure 14: Retraction Test with (a) Stringing and (b) No Stringing

In a retraction test, the figure to be printed will have 2 or more poles or peaks near each other. Starting at zero distance, the test will be printed, and the stringing will be evaluated, increasing by 1 mm each test. No retraction distance prints the worst stringing. If the distance is too high the filament can be pushed out of the driver, take too long to extrude, or clog the nozzle. A good rule to follow is to set the retraction distance no greater than the length of the nozzle. Figure 14, illustrates one retraction test with stringing and one test without [41].

Figure 15: Calibration Cube

Dimensional accuracy determines the outcome of the appearance and tolerances. The accuracy depends on the parameters used and the filament [42]. A calibration cube, shown in Figure 15, is used to check the actual printed dimensions against the model dimensions. This aids in achieving maximum precision and accuracy. After the print is complete, compare the print dimensions to those of the model. There are three ways to adjust. First, using Equation 1, the steps per mm is determined. Then the steps are adjusted in the G-code. The second way is to use the scale feature on the slicing software. The print can be increased or decreased by the difference from the actual print and model. Finally, the print models can be designed on CAD software, with the size difference in mind [43].

$$steps = (\frac{e}{o})(s) \hspace{3cm} (1)$$

1: Steps Calculation

Where: e = expected dimension, o = observed dimension, and s = current number of steps per mm.

Once the parameters above have been determined using their associated tests, a series of calibration tests must be executed to verify the capabilities of the printer. There are many types of calibration tests available. Some test for tolerance, accuracy, stringing, or combine many different tests together.
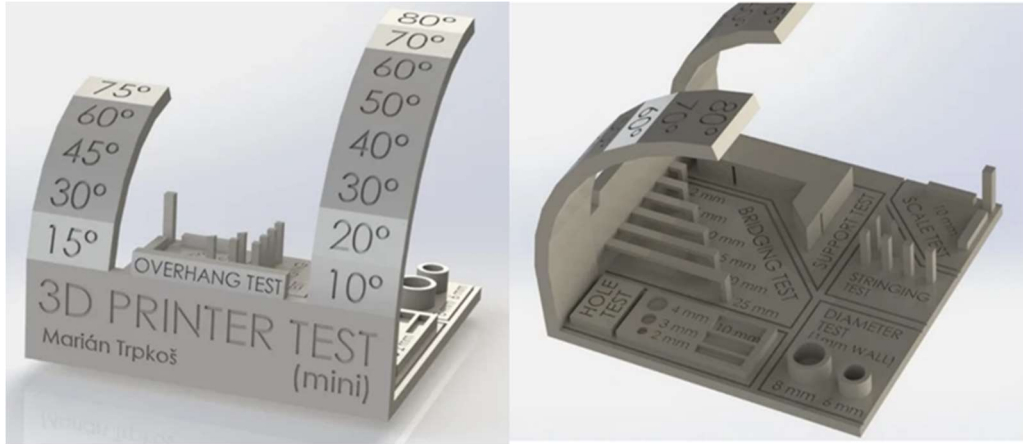
Figure 16: Calibration Test STL

A combined calibration test was chosen. This test contains two overhang tests, one by 10-degree increments and the other by 15-degree increments. An overhang angle is the angle between a vertical line and the print surface. This test demonstrates the largest angle a print can successfully be printed [44]. The support test demonstrates how well the supports are printed. The bridging test has multiple sizes of bridges. This test exhibits how far horizontally a print can travel without sagging or stringing. When needing to add supports, this is useful information. The hole test has three different sizes and measures how small a hole can be printed. The diameter test prints cylinders with a 1 mm wall and measures how accurately the diameter is printed. The stringing test is similar to the retraction test. There are many poles near each other and will display if any stringing occurs. Finally, the scale test has a rectangle scaled in 3 different orientations and demonstrates how accurate each scale is [45].

3.2 PRINTING PARAMETERS

Table 3: Optimized Zytel Printing Parameters

Printing Parameter	Value	Printing Parameter	Value
Layer Height (mm)	0.1	Solid Infill Top	YES
Extrusion Width (mm)	0.4	Solid Infill Bottom	YES
Perimeters	1	Retraction	YES
Flow (%)	100	Initial Layer Thickness (mm)	0.1
Top Layers	4	Initial Layer Flow (%)	100
Bottom Layers	4	Cut Off Object Bottom (mm)	0
Fill Density (%)	100	Travel Speed (mm/s)	55
Print Speed (mm/s)	50	Bottom Layer Speed (%)	30
Printing Temperature (°C)	260	Solid Layer Speed (%)	80
2nd Nozzle Temperature (°C)	0	Outer Shell Speed (%)	75
Print Bed Temperature (°C)	100	Inner Shell Speed (%)	90
Support Type	NONE	Infill Speed (%)	100

Table 4: Retraction Settings

Printing Parameter	Value	Printing Parameter	Value
Speed (mm/s)	20	Minimal Extrusion Before Retracting (mm)	0.001
Distance (mm)	2	Z Hop When Retracting (mm)	0
Minimum Travel (mm)	0.01	Enable Combing	ALL

After following the procedure discussed in section 3.1, the fully optimized printing parameters and retraction settings can be found in Table 3 and Table 4. The material extrusion process is dependent on multiple printing parameters which can be classified into three categories, geometry based, process based, and structural based [46]. Geometry based parameters include nozzle size and filament size. Nozzles range in size from 0.1 to 2.0 mm in diameter, with 0.4 mm being the most commonly used today. The filament sizes offered for material extrusion most commonly are 1.75 mm and 2.85 mm, often referred to as 3 mm filament.

Process based parameters include the nozzle temperature, bed temperature, and printing speed. The nozzle temperature is the temperature at which the molten filament is extruded at. Too hot of a nozzle temperature will result in burning and stringing and blobs due to the filament being too runny and flowing out in an uncontrolled fashion. The nozzle being too cold results in the filament not melting properly forcing a buildup of pressure in the nozzle which leads to the extruder skipping. When the print bed is too hot, it can lead to the initial layers melting resulting in elephant's feet, where the weight of the upper layers forces the initial layers to push out. When

the bed is too cold, issues with adhering are encountered. Print speed determines how fast the printer motors move. A fast print speed can result in the filament being stretched when being printed as the material is being pulled out rather than extruded. A slow print speed may result in deformations as the nozzle can sit on the part for too long.

Structurally based parameters include layer thickness, infill geometry, infill density, raster angle, and raster gap. Layer thickness is the movement in the z-axis between each layer. Infill geometry refers to the pattern that is seen inside of the component. Depending on the slicer software being employed, prints can be programmed to have different infill geometries in different areas of the print. The traditional infill patterns include triangular, rectilinear/grid, hexagonal, and wiggle. Infill density is the amount of material that is inside of the component. This percentage ranges from 0 percent (hollow) to 100 percent (solid), which has an effect on the overall strength of the component. The raster angle is the angle between the nozzle direction with respect to the x-axis. Normal raster angles include 0°, 45°, and 90°. Choosing a raster angle depends on the intended service application as different angles provide different strengths. Finally, raster gap is simply the space between two adjacent filament deposits.

3.3   BUILD QUALITY
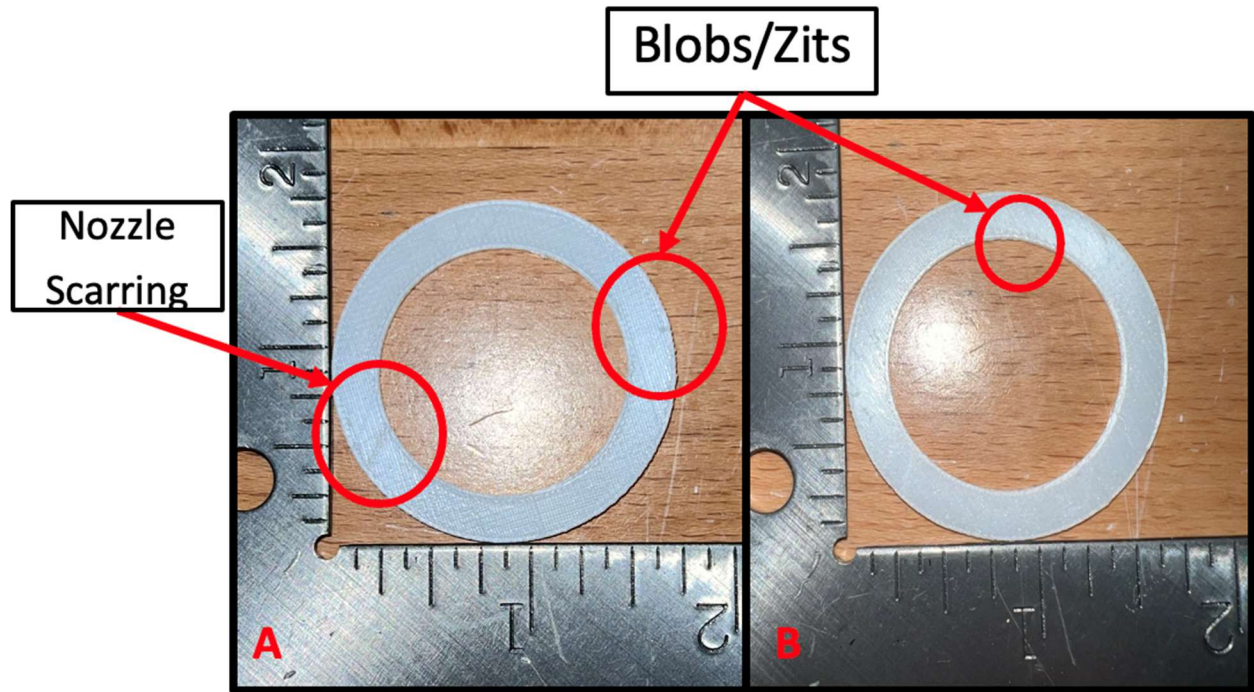
Figure 17: ASTM F37B Gasket Specimen (A) Top and (B) Bottom Surface
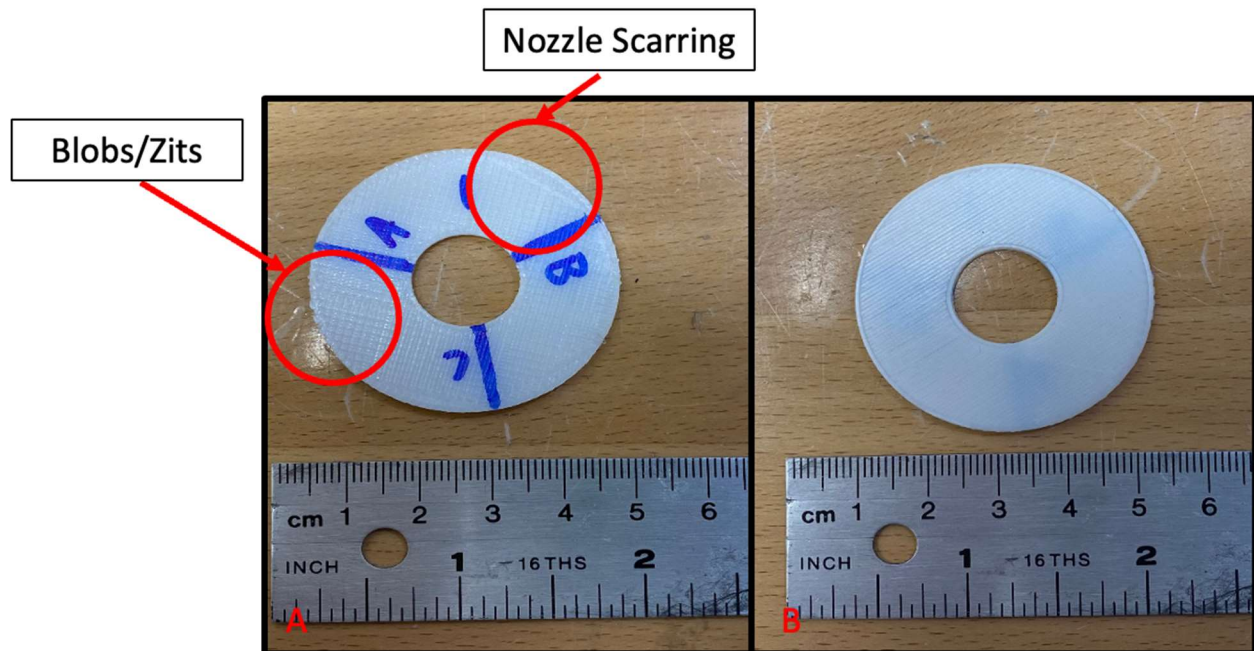
Figure 18: ASTM F38B Gasket Specimen (A) Top and (B) Bottom Surface

Representative images of the top and bottom surfaces of both ASTM F37B and ASTM F38B test specimens are seen in Figure 17 and Figure 18 respectively. Although the printing parameters have been optimized as elaborated in section 3.2, very minor print imperfections can still arise. The two most common imperfections seen in the manufactured specimens are blobs, also known as zits, and nozzle scarring. The blobs that do result from printing, are located on both the inner and outer diameters. The overhang material on the edges doesn't pose any risk to the performance of the gasket except in cases where tight tolerances are of concern. If the blobs do become an issue for tolerance, simple post processing with a Dremel tool or medium grit sandpaper can easily resolve the issue. Nozzle scarring occurs when the print bed is slightly off level or the z-axis offset calibrated prior to printing may be off by a few microns resulting with the nozzle being too close to the print bed. The print bed being slightly not level may cause the operator to assume the z-axis offset is incorrect and the issue will not be resolved. The issue can easily be resolved if the print bed is first leveled and then checked to see if the nozzle scarring issue is still present. Most of the time, an uneven print bed is the root cause because the print bed can easily become unlevel as prints are completed. The nozzle scarring issue does not pose a significant threat to the build integrity of the gaskets if the issue is minor.

4 TEST MATRIX AND TEST METHODS

4.1 THERMAL SOAK

Figure 19: Gaskets in Tenney Environmental Chamber for Thermal Soak

A thermal soak at the target temperatures prior to sealability testing is required as the capabilities to conduct the tests at temperature is not available at the laboratory. The gaskets were conditioned for twenty-two (22) hours at temperature suspended on a wire rack with no external load applied. This ensures that the specimens are saturated evenly by allowing chamber air to circulate all around the specimen as seen in Figure 19. In order to avoid any discrepancies with different thermal soaks at the same isotherm, all of the specimens were soaked together.

4.2   SEALABILITY (ASTM F37B)

The ASTM standard being employed is ASTM F37, test method B. ASTM F37 is the standard for testing the sealability of gasketing materials. Test method B specifically tests the material ability to seal a gas medium, dry nitrogen was used for this study [47]. The testing panel and load cell can be seen in Figure 9. To begin the test, a conditioned gasket will be placed concentrically to the center hole of the smooth bottom platen. The top platen is placed on top of the gasket and then bolted on with an eleven-millimeter (11.0 mm) diameter load transducer followed by a dial indicator to display how much load is being applied. Once the cell cage is assembled, the test procedure is ready to begin. The first step in the test is to apply the desired load by using the tick marks on the dial indicator by tightening the four bolts by an equal amount of turning. This step requires the load to be applied in less than one minute. Once the load is applied, the load should not be lowered by any means until the test is completed, even if the load is slightly higher than intended. The system must be pressurized slowly by opening the regulator and allowing the nitrogen to build to an internal pressure of thirty (30) psi. Once the system is pressurized, the system is held untouched for two minutes to allow for the gasket to normalize. Once the time has passed, the test may begin by closing the valve leading to the test cell. The time is taken for the manometer level to increase to the third notch level. Once the third notch is reached, the test is complete and is ready to be reset for the next test. This procedure will be done for the 3 pressures of interest: two (2), four (4), and six (6) MPa. This test gives the information needed to determine the leak rate of the gasket by the change of volume by the duration of time it took, which can be detailed by Equation 2: Leak Rate Equation:

$$Q = \frac{\Delta V}{\Delta t} \qquad\qquad (2)$$

2: Leak Rate Equation

where Q is the calculated leak rate (ml/min), ΔV is the change on volume of the manometer (mL), and Δt is time elapsed (minutes).

Table 5: ASTM F37B Test Matrix

Temperature (°C)	# Of Specimen	Load (MPa)	Internal Pressure (psi)
-55°C	3	2	30
-55°C	3	4	30
-55°C	3	6	30
22°C	3	2	30
22°C	3	4	30
22°C	3	6	30
100°C	3	2	30
100°C	3	4	30
100°C	3	6	30

The test matrix for the sealability testing according to ASTM F37B is seen in Table 5. There will be 3 samples tested for each isotherm at each pressure load of interest. This means that thirty-six individual tests will be conducted to fulfill the test matrix. The information to be obtained from this study is both the effects of thermal soaking at high and low temperatures. The other output expected is to determine the pressure load that yields the lowest leak rate value.

4.3   CREEP RELAXATION (ASTM F38B)
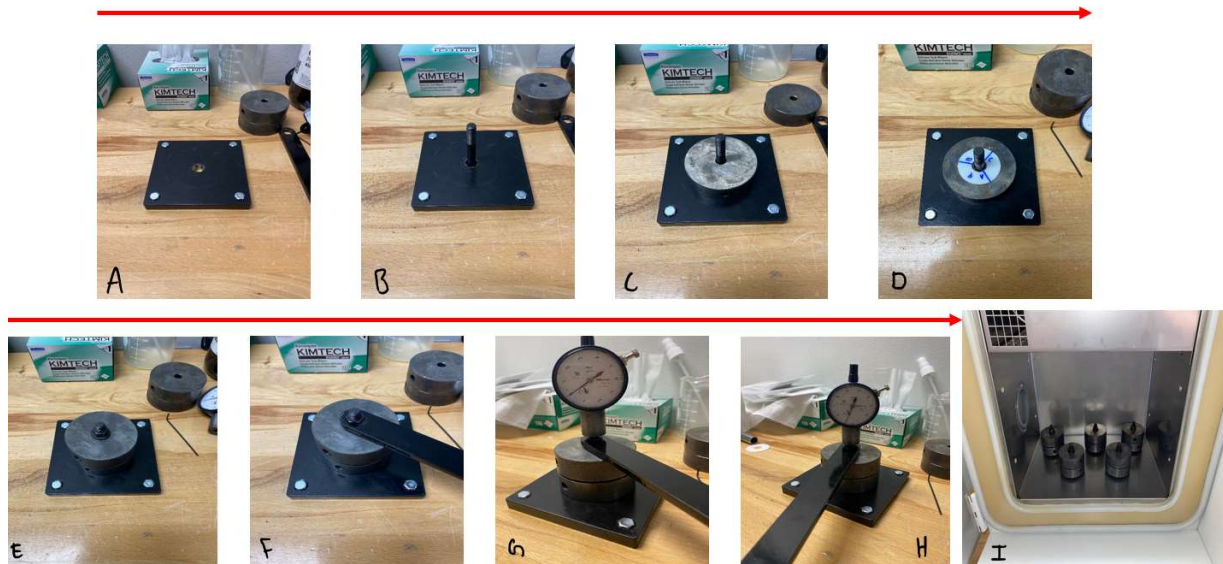
Figure 20: The Process of Test Setup for Each Sample for ASTM F38B

The creep relaxation of the gasket material is evaluated according to ASTM F38 [48]. No specific material or environmental requirements are stated in the standard. The loading process of each specimen can be seen in Figure 20. The standard calls that the annular test specimen is placed concentric to the tightening bolt in order to ensure that there is an even distribution of stress on the gasket (Figure 20D). When the top platen is placed and the nut is finger tight, the tightening wrench and dial indicator are placed on the assembly (Figure 20G). The dial indicator is zeroed simply by rotating the dial's face to "0". While tightening the bolt assembly, the dial indicator must be monitored in order to not over/under tighten the nut. For this series of testing, a total compressive stress of 2 MPa is used which equates to a total displacement of 10 ticks on the dial indicator (D_0). After the platens are thermally soaked, the procedure seen in Figure 20 is simply reversed. When

the bolt assembly is loosened, the final change in the dial indicator reading is noted as D_f. The

creep relaxation of each test specimen is calculated using Equation 3 below:

$$Relaxation\ (\%) = \frac{D_0 - D_f}{D_0} \times 100 \tag{3}$$

3: Relaxation Percentage

Where D_0 is the initial displacement reading (in), and D_f is the final displacement reading (in).

Tests are conducted in quintuplets for each test condition.

Table 6: Initial Tests Test Matrix

Temperature (°C)	Load (MPa)	Hold (hr)	Normalize
-55°C	2	22	2hr/22°C
22°C	2	22	2hr/22°C
100°C	2	22	2hr/22°C

Three different tests were conducted to fulfill this task, each with the intent to further

understand the creep relaxation behavior. The first experiment conducted was the initial testing

based on the ASTM F38B standard. The test matrix can be found in Table 6. This test series

consists of a total of fifteen gaskets tested. Five specimens will be in each test at either -55, 22, or

100°C. Conducting the ASTM standard test at three different isotherms allows for the

understanding of drastically different temperature affect the gaskets.

Table 7: Cold Series Test Matrix

Temperature (°C)	Load (MPa)	Hold (hr)	Normalize

-55°C	2	22	2hr/22°C
-55°C	4	22	2hr/22°C
-55°C	6	22	2hr/22°C

The second series of tests was conducted to further analyze whether thermal contraction is the cause for such high recoverability when compared to the other previously tested isotherms. The series consists of three tests at -55°C, each with a different compressive load of 2, 4, or 6 MPa for twenty-two hours, as seen in Table 7. There is a total of fifteen data points collected from this matrix.
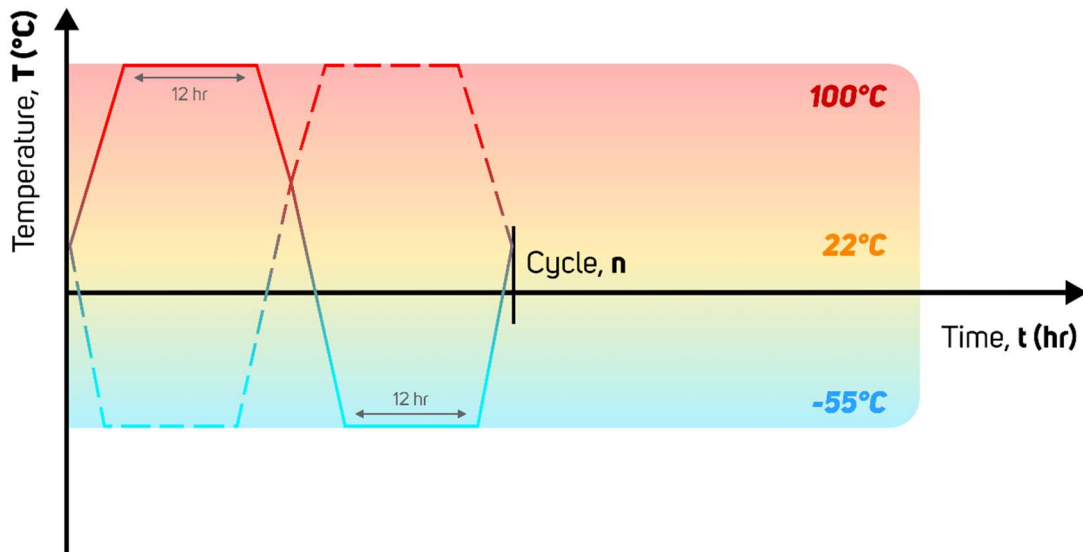
Figure 21: Creep Relaxation Thermal Cycle Schematic

Table 8: Thermal Cycle Test Matrix

ID	Load (MPa)	1st Step	2nd Step	Hold (hr)	# Of Cycles	Normalize
Hot/Cold	2	100°C	-55°C	22	7	2hr/22°C
Cold/Hot	2	-55°C	100°C	22	7	2hr/22°C

The third and last series of testing done were extended thermal outlined in Table 8. Each thermal cycle consists of two 12-hour steps, each at -55°C or 100°C, which can be visualized in Figure 21. There is a total of 7 cycles completed per test, for a total of 7 days and 2 hours (the normalization period after the cycling). The main difference between the two tests is that one begins with a 100°C step first and the other begins with a -55°C.

5   RESULTS AND DISCUSSION

5.1   SEALABILITY
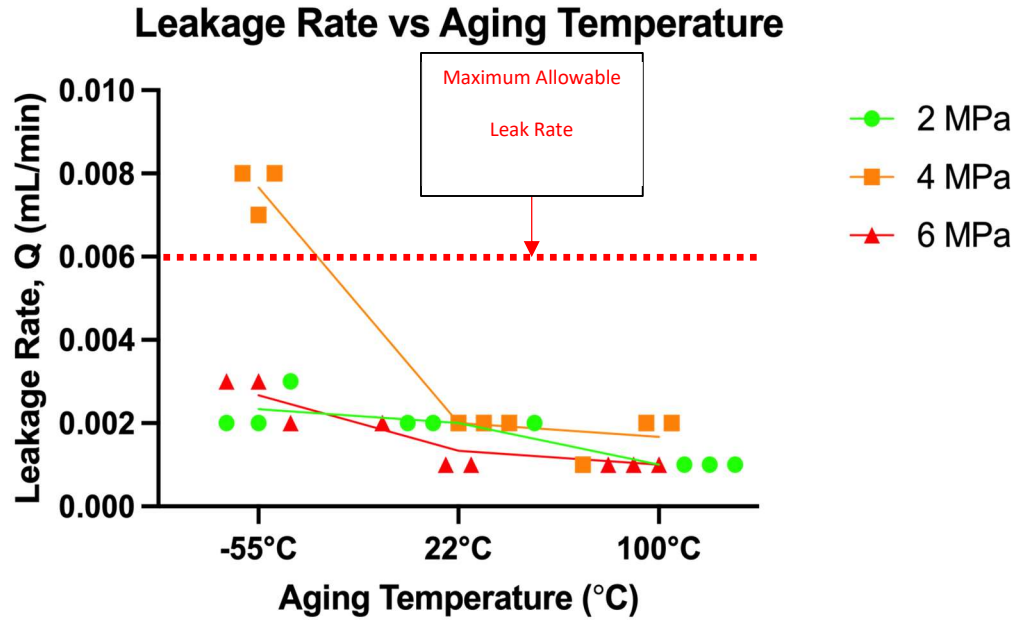
Figure 22: Leakage rate vs Aging Temperature

Table 9: Regression Lines and Equations

Flange Load	Equation Type	Equation	R^2 Value
2 MPa	Linear	$-8.611^{-6x} + 1.97^{-6}$	0.7516
4 MPa	Exponential	$3.632^{-3} * e^{-1.013^{-2x}}$	0.9136
6 MPa	Exponential	$1.711^{-3} * e^{-6.209^{-3x}}$	0.7466

Sealability is reported in Figure 22. The graph plots the thermal soak temperature on the x-axis versus the resultant sealability of the gaskets on the y-axis. There is a red dotted line indicating the maximum allowable leak rate of proton exchange membrane fuel cells [26]. The provided legend indicates the flange load. There is overlapping test data which indicates the reliability of the gaskets. The equations of the regression lines for the data are found in Table 9. The equations are a function of the applied thermal soak in and how that affects the resultant leak rate. The optimal outcome of sealability would be indicated by the lower leak rate, high leak rates suggest poor sealability.

There is a trend of decreasing leak rate when increasing the thermal soak temperature. The room temperature specimen had an average leak rate of 0.002 mL/min, which acts as baseline for comparing the data. The 100°C thermal soak resulted in a significantly lower leak rate when comparing the other aging temperatures with an average leak rate of 0.001 mL/min, the lowest leak rate recorded across all experiments. The -55°C thermal soaked specimen performed the worst of all isotherms with an average leak rate of 0.0042 mL/min. It is evident that a thermal soak plays a crucial role in the sealability performance of the specimen.

Flange load saw an interesting trend where the low and high loads, 2 and 6 MPa respectably, resulted in superior compared to those of the mid-rage flange load of 4 MPa. Overall, the flange load of 6 MPa, which translates to 0.0005 inches of compression, yielded the lowest average leak rate of 0.0017 mL/min. The biggest concern about using a higher compressive load is that the material may degrade faster or even reduce the functionality of the entire PEMFC as a whole [19,20]. A 2 MPa flange load delivered an average leak rate of 0.0018 mL/min, which while slightly higher than 6 MPa results, may prove that a higher flange load does not directly translate into a significantly better leak rate. The flange load of 4 MPa had an average leak rate of 0.0038

mL/min which is significantly greater in comparison to the other flange loads. What was expected to see from 4 MPa being the intermediate load of the three tested flange loads was for the leak rates to be comparable or in-between the other flange loads. Further analysis via XCT is still required to determine the reasoning for occurrence.

When evaluated together, it is evident that a 100°C thermal soak and a flange load of 2 MPa produced the best leak rates. This is derived from the decreasing trendlines seen in Figure 22 across all three flange loads. The highest average leak rate of 0.0077 mL/min was a result of the -55°C thermal soak and a flange load of 4 MPa. Overall, it is evident that 100°C thermal soak produced the lowest leak rates of all the specimen at all three pressure levels which suggests that during the thermal soak, build defects are corrected resulting in a better sealability. Comparing the data experimental data obtained in the experiments to the maximum allowable leak rate put forth by Borup [26], it is evident that the sealability of material extruded Zytel meets the initial leak rate criteria. The only samples to exceed the maximum allowable leak rate were the -55°C thermal soaked specimen at a flange load of 4 MPa. This is due to the thermal damage that is onset during the soak such as cracks and voids being opened acting as pores for gas to escape or stress concentrations that then intern create voids due to the flange compression.

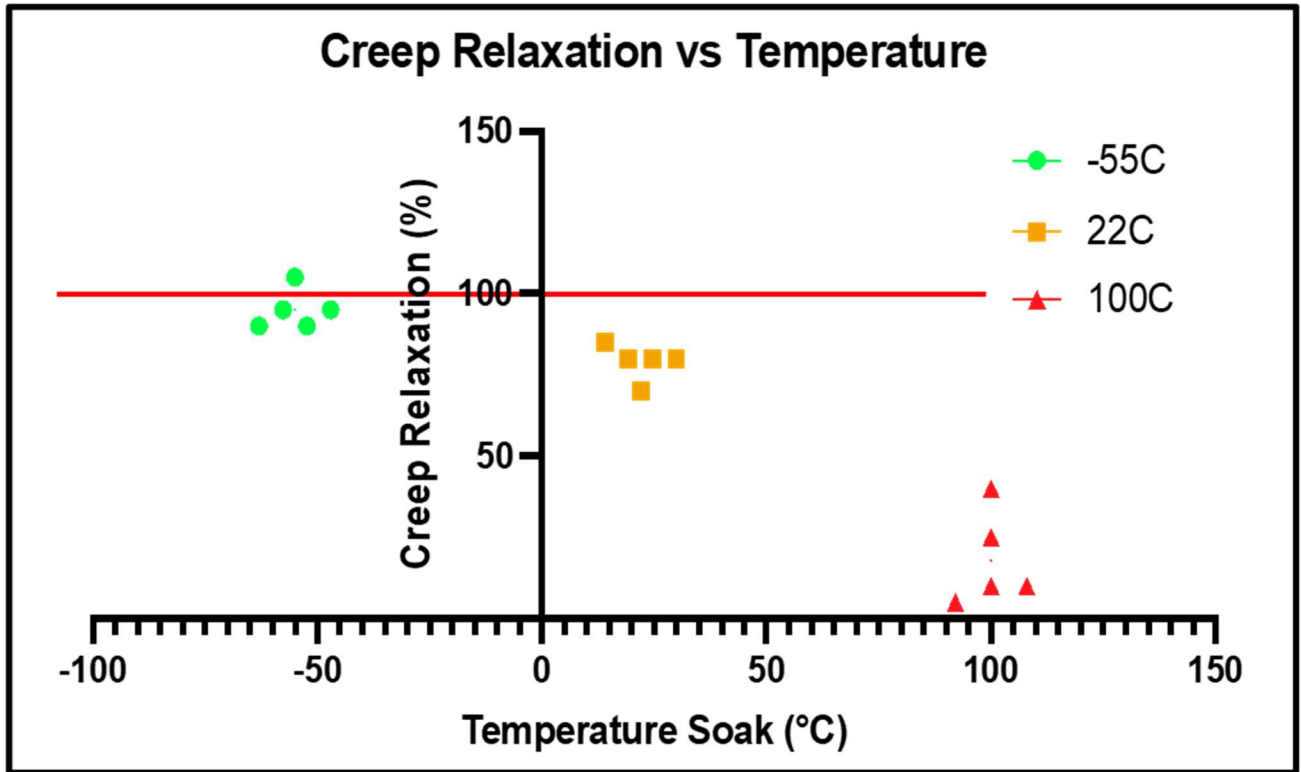## 5.2 CREEP RELAXATION

5.2.1 INITIAL TESTING

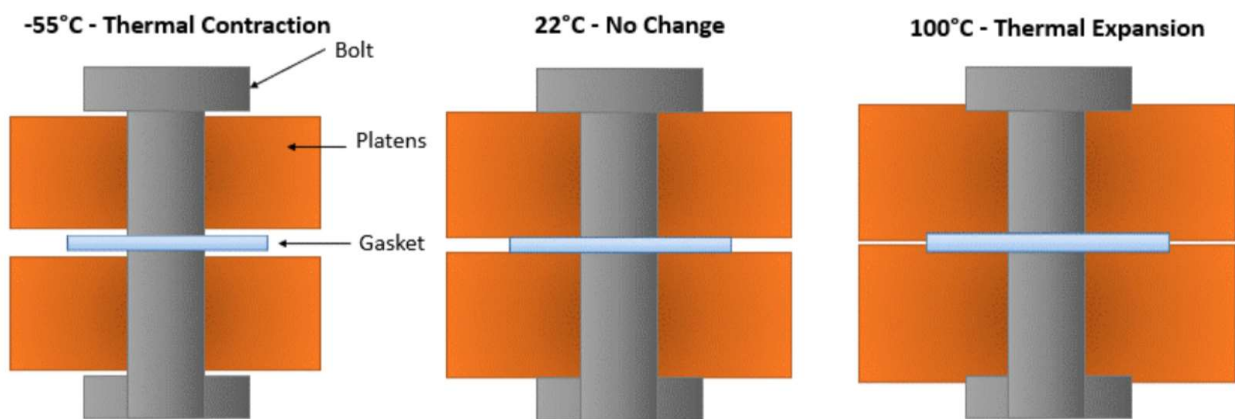Figure 23: Recoverability Results of Testing at 2 MPa

Figure 24: Thermal Contraction and Expansion Hypothesis

The recovery results of the 22-hour tests at -55, 22, and 100°C with a 2 MPa compressive load can be found in Figure 23. The red line on the graph represents the maximum recoverability that the material can experience, which is 100%. It is evident that temperature plays a massive role on how the material behaves, even with a short 22-hour test. The cold series, tested at -55°C, displayed the highest recoverability percentage with an average recoverability of 95%. On the other end, the hot series, tested at 100°C, produced the lowest recoverability results with an average of 18%. The room temperature series, tested at 22°C, yielded an average recoverability of 79%, significantly better than the hot series. When analyzing all the data, it is evident that the results follow an exponential regression behavior reaching an asymptote at -55°C. As temperature increases, the maximum recoverability also decreases. The decrease is very slow until 22-25°C where the rate at recoverability decreases drastically, hence the exponential regression behavior. It is hypothesized that thermal expansion and compression is the cause for such a drastic difference in recoverability between a low temperature test and high temperature test.

An over exaggerated schematic of the hypothesis is seen in Figure 24. It is not concluded whether the thermal contraction and expansion is occurring in the whole system (i.e., the platens, gasket, and tightening bolt) or a singular component. At extreme cold temperatures, thermal contraction causes the compressive load to either lose partial load or lose it entirely. This would mean that the gasket is simply sitting in the -55°C environment with only the weight of the top platen acting on the gasket. Once the system returned to temperature and the contraction equalizes, the compressive load is regained again. During this 2-hour period, this is likely the only time the gasket has the initial full load applied to it which, which is why the experiment still yields the 95% recoverability. Like the cold soaks, it is unknown whether the entire system or just the gasket is expanding during the high temperature tests. In combination with thermal expansion, annealing is

also playing a role in the low recoverability. Annealing is the process of recrystallizing the crystals in a polymer increase the overall strength of the polymer. As a result of annealing, the shape of the polymer can be changed. Due to the combination of thermal expansion and annealing caused at 100°C, the recoverability of the gasket is greatly affected.

5.2.2   COLD SOAK SERIES
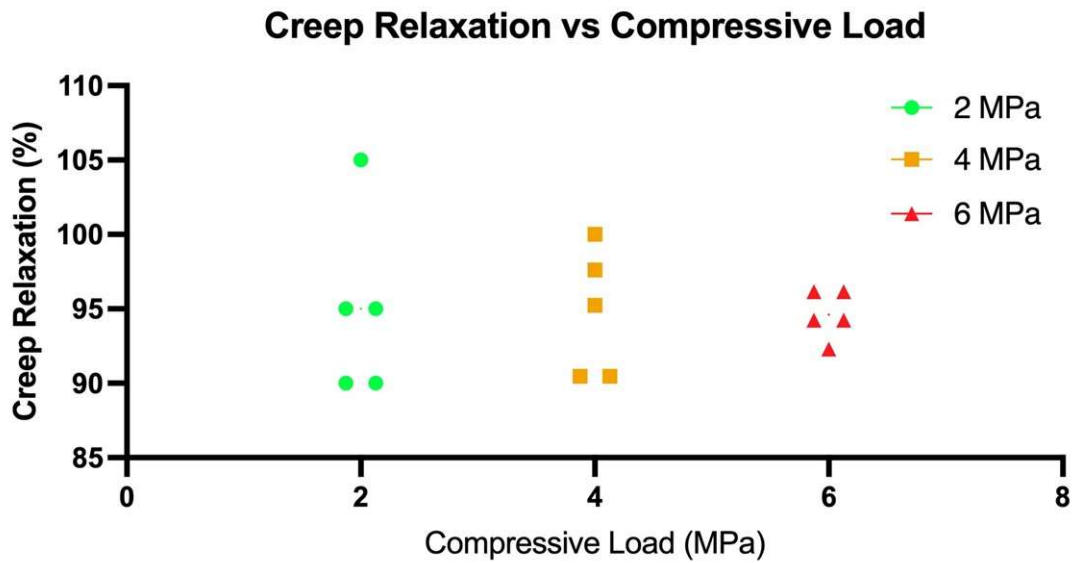
Figure 25: Cold Soak Series Results

To further investigate whether thermal contraction was occurring at -55°C, a series of tests were completed at varying compressive loads at -55°C. The results of the tests are shown in Figure 25. From the results, thermal contraction is the cause for the high recoverability percentages. The average recoverability of the original test at 2 MPa was 95%. The average recoverability of the 4 and 6 MPa tests were 94.76% and 94.62% respectively. The very slight decreases in recoverability are a result of the higher compressive loads being applied to the gasket during the two-hour recoverability period. The precision of the data did increase as the compressive loads increased, meaning that the data is more reliable. Thermal contraction affects the system by significantly

reducing the applied load or it zeroes it to where the weight of the top platen is the only force during that time. This phenomenon is not ideal as if this were to occur in a live fuel cell environment, the gasket would completely fail due to crossover leakage and leakage out of the cell itself. Shrinkage occurring at any point during operation could pose a loss of efficiency, loss of property, and a safety hazard as hydrogen and oxygen gasses are highly flammable.

5.2.3 THERMAL CYCLE
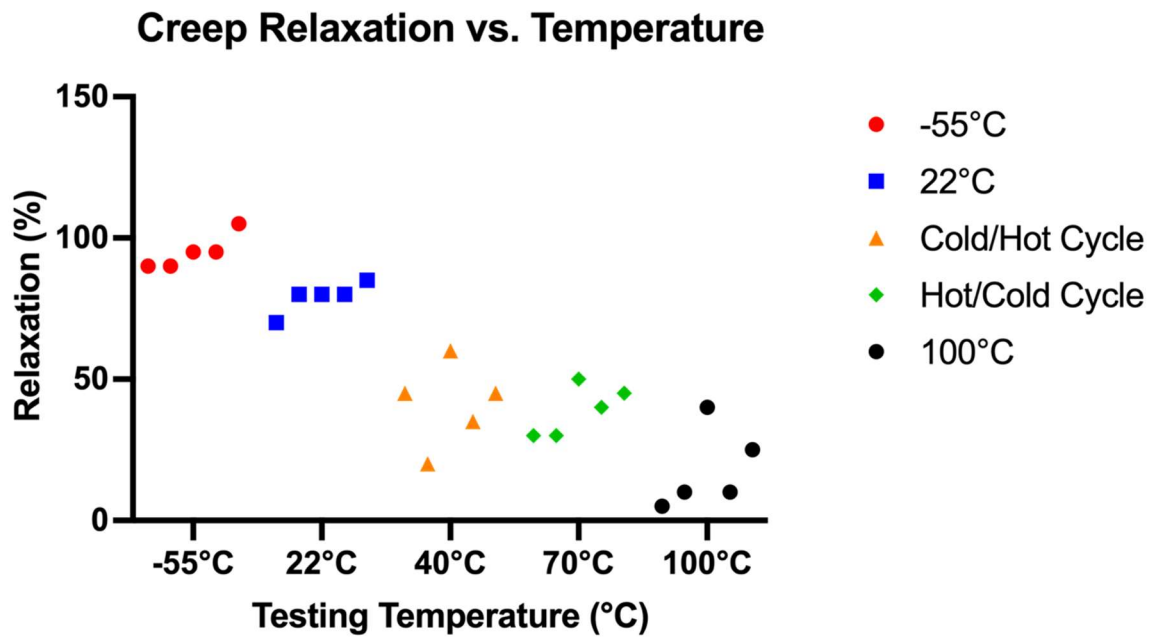
Figure 26: Temperature Cycle Results Next to Initial Tests

To investigate how the Zytel gaskets perform under a long-term thermal cycle, two 7-day thermal cycles ranging between -55 and 100°C were conducted. The difference between the two thermal cycles is that one soaked at 100°C first then cycled to -55°C and the other started at -55°C and then cycled to 100°C. Doing this allowed the determination whether they produced drastically different recoverability results. The results of the two thermal cycles can be seen in Figure 26 compared to the results of the thermal soaks in section 5.2.1. The results of the thermal cycles are

comparable to each other with the cold first thermal cycle having an average 41% recoverability and the hot first thermal cycle had a 39% average recoverability. It appears that the Zytel gaskets normalize at around 40% recoverability with an original loading of 2 MPa. The difference between the different thermal cycles lies in the precision of the five tested samples. The hot-first thermal cycle had a standard deviation of 8% while the cold first thermal cycle yielded a standard deviation of 13.19%. This is a direct result of the cold-first thermal cycles having 2 outlier data points, one higher and one lower percent recoverability that average out to 40%.

It is hypothesized that this is a result of the gaskets being annealed and reshaped first rather than soaking at -55°C with a very minimal load for the first 12 hours of thermal cycle. Considering that the material being used is classified as a thermoplastic that is typically more susceptible to higher compression set (lower recoverability percentages), an average of 40% is a promising value. More work is required to determine the true creep relaxation values in service.

5.3   X-RAY DIFFRACTION ANALYSIS
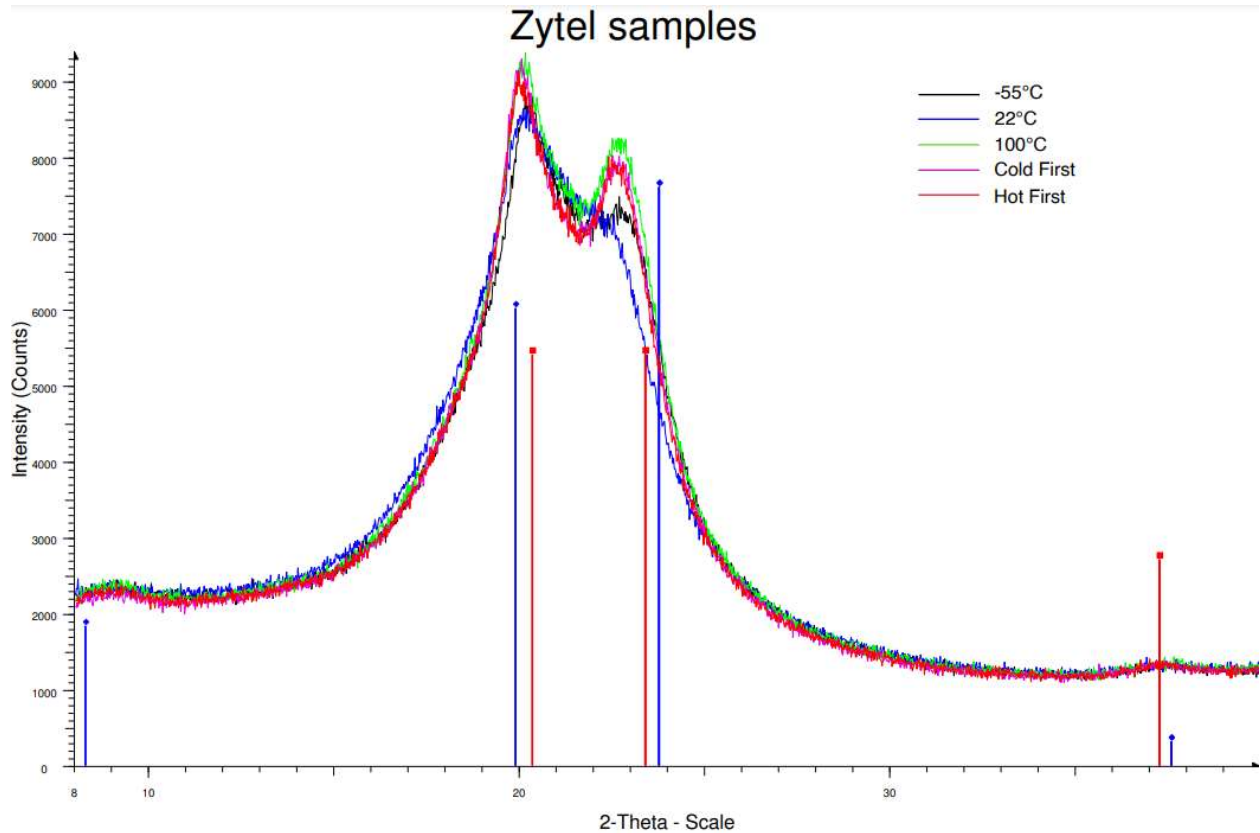
Figure 27: XRD Results of Scanned Zytel Specimen

The resultant x-ray diffraction graph from the Zyel gaskets can be seen in Figure 27. The 2-theta angle is plotted against the recorded intensities. It is observed that four distinct peaks are present, two at lower intensities and two at significantly higher intensities. The two lower intensity peaks occur at approximately 9° and 37° degrees while the two high intensity peaks occur at 20° and 23° degrees. The spectra produced by Zytel is consistent with that of a semicrystalline thermoplastic and Zytel with a medium to high degree of crystallinity [51-53]. There are two distinct grouped bands, group "A" consists of 100°C, Cold First, and Hot First spectra while group "B" is made up of the -55°C and 22°C spectra. This was the expected results based on the hypothesis of annealing

occurring. Group "B" displayed a greater intensity at the peaks at 20° and 23°. It can be concluded that the samples that were exposed to a temperature of 100°C, whether during a thermal cycle or thermal soak, were annealed slightly based upon the slight increase in peak intensities coupled with the sharper peaks visible at 20°.

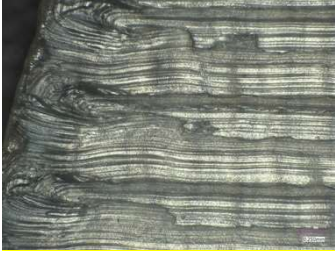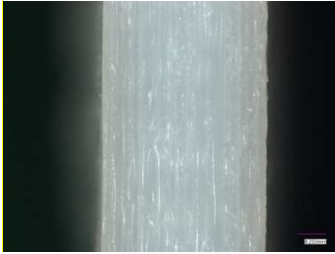## 5.4 MICROSTRUCTURAL ANALYSIS

	(a)	(b)	(c)
Top			
Side			
Bottom			

Table 10: Digital Microscopy at 100x magnification of specimen Post thermal soak at (a) -55°C

(b) 22°C (c) 100°C

Optical microscopy images of the AM Zytel specimen are shown in Table 10. The images were taken in the top, side, and bottom orientations after thermally soaking at the target temperatures of -55, 22, and 100°C. It was observed that the gaskets soaked at 100°C developed a light yellowish tinge on all sides, not pictured in Table 10, due to being exposed to a high temperature for a prolonged period of time. The color of the other specimen tested at -55°C and 22°C remained unchanged. The raster pattern can easily be seen on the top surface of all the gaskets displaying no visible signs of damage post thermal soak. Although the gaskets were printed with a 45° raster angle, they were imaged to present with a 0° or horizontal raster angle. When analyzing the side profiles of the gaskets, no delamination or layer warpage was observed across all specimens. The absence of delamination is indicative that the material is stable in the environment, without the application of external forces. Debris in the form of fibers, hairs, and small plastic particles from the air can be seen entrapped on the surfaces as well as in-between the layers. The debris does not pose a direct issue to the integrity of the gaskets themselves. It was observed that some of the residual glue from the print bed remained on the bottom side of the -55°C and 22°C gaskets. Although the specimens are cleaned with soap and water after printing in order to remove the residual glue, some still remains. The residual glue on the 100°C thermal soaked specimen appears to be baked into the bottom face of the gaskets, highlighting the geometry created by the fused layers and the inter-fiber bonding regions created during the first layers of a print.

6   CONCLUSIONS AND FUTURE WORK

6.1   CONCLUSIONS

The main concern for these additively manufactured components is their ability to seal after being exposed to extreme temperature environments. The first objective was to evaluate how a thermal soak affects the material's ability to maintain a seal compared to the room temperature condition. Through the testing of these isotherms, there is a clear trend observed where the -55°C thermal soak resulted with higher leak rates (poorer sealability) compared to the 100°C thermal soak specimen that had lower leak rates (better sealability). It is concluded that the hot thermal soak improves the sealability of these gaskets across all three flange loads. This is likely due to the 100°C thermal soak correcting existing build defects of printing. The second objective was to determine the pressure that results in the lowest leak rate. Two pressure levels, 2 and 6 MPa load, produce lower leak rates compared to a 4 MPa load. This is hypothesized to be due to microscopic damage caused by the higher compressive load that creates openings for the nitrogen gas to leak out of. Although 6 MPa has a higher compressive load, the higher load likely corrects some of the damage initiated during compression. Using a high load of 6 MPa can lead to accelerated degradation and cause the fuel cell to lose efficiency or even failure of the fuel cell.

Zytel's creep relaxation behavior appears to be affected more by temperature than time. When the gaskets were all tested for 22 hours at temperature, Zytel exhibited an exponential regression behavior with respect to temperature. As temperature increased from -55°C to 22-25°C, the maximum percent recoverability decreased slowly. After 25°C, the maximum recoverability decreases rapidly to 100°C. It was concluded that thermal contraction is causing the loss of load at cryogenic temperatures which is not ideal in a fuel cell environment. When the Zytel gaskets

underwent two different seven-day thermal cycles, they averaged 40% recoverability. To ensure precision in the performance of the Zytel gaskets, starting at a higher temperature will help.

6.2   FUTURE WORK

The largest gap left to be investigated is Zytel's sealability with hydrogen gas as the medium. Unfortunately, the laboratory where the work was conducted is not outfitted for hydrogen use. Installing an in-line pressure digital pressure gauge onto the sealability testing assembly will allow for a more accurate tracking of pressure loss compared to using the standard manometer. Zytel's chemical resistance also needs to be measured. This could be facilitated by conducting a similar series of experiments seen in Wei Lin et al. [21], where the specimens are submerged in an accelerated aging solution and allowed to thermally cycled. It would be possible to conduct creep relaxation experiments in the aging solution at temperature. Ultimately it would be ideal to fabricate gaskets and assemble them into a fuel cell and record how the gasket performs.

7   REFERENCES

[1] Kar, S. K., Harichandan, S., & Roy, B. (2022). Bibliometric analysis of the research on hydrogen economy: An analysis of current findings and roadmap ahead. International Journal of Hydrogen Energy

[2] Moriarty, P., & Honnery, D. (2009). Hydrogen's role in an uncertain energy future. international journal of hydrogen energy, 34(1), 31-39.

[3] Dillman, K., & Heinonen, J. A 'Just'Hydrogen Economy: A Normative Energy Justice Assessment of the Hydrogen Economy. Available at SSRN 4081111.

[4] IEA. (2021, October). Global Hydrogen Review 2021 – Analysis. IEA. Retrieved August 2022, from https://www.iea.org/reports/global-hydrogen-review-2021

[5] Griffiths, S., Sovacool, B. K., Kim, J., Bazilian, M., & Uratani, J. M. (2021). Industrial decarbonization via hydrogen: A critical and systematic review of developments, socio-technical systems and policy options. Energy Research & Social Science, 80, 102208.

[6] Energy Transitions Commission. (2020). Making mission possible: Delivering a net-zero economy. Energy Transitions Commission. https://www. energytransitions. org/publications/making-mission-possible.

[7] Council, H. (2017). Hydrogen scaling up: A sustainable pathway for the global energy transition.

[8] Net Zero by 2050 – Analysis. IEA. (2022, June). Retrieved August 2022, from https://www.iea.org/reports/net-zero-by-2050

[9] Barbir, F. (2013). Pem Fuel Cells Theory and Practice (2nd ed.). Elsevier/Academic Press.

[10] Ramani, V. (2006). Fuel Cells - Electrochemical Society. Fuel Cells. Retrieved March 2022, from https://www.electrochem.org/dl/interface/spr/spr06/spr06_p41-44.pdf

[11] Husar, A., Serra, M., & Kunusch, C. (2007). Description of gasket failure in a 7 cell PEMFC stack. *Journal of power sources*, *169*(1), 85-91.

[12] Blakey-Milner, B., Gradl, P., Snedden, G., Brooks, M., Pitot, J., Lopez, E., ... & du Plessis, A. (2021). Metal additive manufacturing in aerospace: A review. Materials & Design, 209, 110008.

[13] Leal, R., Barreiros, F. M., Alves, L., Romeiro, F., Vasco, J. C., Santos, M., & Marto, C. (2017). Additive manufacturing tooling for the automotive industry. The International Journal of Advanced Manufacturing Technology, 92(5), 1671-1676.

[14] Skardal, A., & Atala, A. (2015). Biomaterials for integration with 3-D bioprinting. Annals of biomedical engineering, 43(3), 730-746.

[15] Alexander, David, "Suitability of Low-Cost Additive Manufacturing for Polymer Electrolyte Fuel Cells" (2022). Open Access Theses & Dissertations. 3469.

https://scholarworks.utep.edu/open_etd/3469

[16] Yuan, X. Z., Nayoze-Coynel, C., Shaigan, N., Fisher, D., Zhao, N., Zamel, N., ... & Groos, U. (2021). A review of functions, attributes, properties and measurements for the quality control of proton exchange membrane fuel cell components. Journal of Power Sources, 491, 229540.

[17] Qiu, D., Liang, P., Peng, L., Yi, P., Lai, X., & Ni, J. (2020). Material behavior of rubber sealing for proton exchange membrane fuel cells. International Journal of Hydrogen Energy, 45(8), 5465-5473.

[18] Spiegel, C. (2017, October 24). Fuel Cell Gaskets, Spacers, and End Plates. Fuel Cell Store. Retrieved 2022, from https://www.fuelcellstore.com/blog-section/fuel-cell-gaskets-spacers-and-end-plates

[19] Lebrun, G., & Denault, J. (2010). Effect of annealing on the thermal expansion and residual stresses of bidirectional thermoplastic composite laminates. Composites Part A: Applied Science and Manufacturing, 41(1), 101-107.

[20] Schulze, M., Knöri, T., Schneider, A., & Gülzow, E. (2004). Degradation of sealings for PEFC test cells during fuel cell operation. Journal of Power Sources, 127(1-2), 222-229.

[21] Lin, C. W., Chien, C. H., Tan, J., Chao, Y. J., & Van Zee, J. W. (2011). Dynamic mechanical characteristics of five elastomeric gasket materials aged in a simulated and an accelerated PEM fuel cell environment. international journal of hydrogen energy, 36(11), 6756-6767.

[22] Tan, J., Chao, Y. J., Wang, H., Gong, J., & Van Zee, J. W. (2009). Chemical and mechanical stability of EPDM in a PEM fuel cell environment. Polymer degradation and stability, 94(11), 2072-2078.

[23] Tan, J., Chao, Y. J., Yang, M., Lee, W. K., & Van Zee, J. W. (2011). Chemical and mechanical stability of a Silicone gasket material exposed to PEM fuel cell environment. International journal of hydrogen energy, 36(2), 1846-1852.

[24] Shen, L., Xia, L., Han, T., Wu, H., & Guo, S. (2016). Improvement of hardness and compression set properties of EPDM seals with alternating multilayered structure for PEM fuel cells. International Journal of Hydrogen Energy, 41(48), 23164-23172.

[25] 3.4 Fuel Cells - Energy. (n.d.). Retrieved February 2022, from https://www.energy.gov/sites/default/files/2017/05/f34/fcto_myrdd_fuel_cells.pdf

[26] Borup, R. L., & Vanderborgh, N. E. (1995). Design and testing criteria for bipolar plate materials for PEM fuel cell applications. MRS Online Proceedings Library (OPL), 393.

[27] Dupont Performance Polymers Zytel®. (n.d.). Retrieved July 8, 2020, from http://matweb.com/search/DataSheet.aspx?MatGUID=5241fee531a9448d9f6f91317f51e4c8

[28] Ethylene Propylene Rubber (EPM, EPDM). Ethylene propylene rubber (EPM, EPDM). (n.d.). Retrieved July 8, 2020, from http://matweb.com/search/DataSheet.aspx?MatGUID=f8e3355cc2c541fbb0174960466819c0

[29] Overview of materials for polytetrafluoroethylene (PTFE). (n.d.). Retrieved July 8, 2020, from

http://matweb.com/search/DataSheet.aspx?MatGUID=4e0b2e88eeba4aaeb18e8820f1444cdb

[30] PTFE and Teflon Chemical Compatibility Chart. CP Lab Safety. (n.d.). Retrieved July 8, 2020, from https://www.calpaclab.com/teflon-ptfe-compatibility/

[31] Tan, J., Chao, Y., Van Zee, J. and Lee, W., 2007. Degradation of elastomeric gasket materials in PEM fuel cells. Materials Science and Engineering: A, 445-446, pp.669-675.

[32] Fluorosilicone rubber (FMQ, FVMQ, FSI). (n.d.). Retrieved July 8, 2020, from http://matweb.com/search/DataSheet.aspx?MatGUID=5a39836207ff4b72acc19d1ab8099830

[33] Dupot Zytel 3D1000FL datasheet.

[34] Dupot Zytel 3D1000FL handling and printing guide

[35] DuPont Material Solutions for Fuel Cell Systems

[36] Spoerk, M., Holzer, C., & Gonzalez-Gutierrez, J. (2020). Material extrusion-based additive manufacturing of polypropylene: A review on how to improve dimensional inaccuracy and warpage. Journal of Applied Polymer Science, 137(12), 48545.

[37] Xiaoyong, S., Liangcheng, C., Honglin, M., Peng, G., Zhanwei, B., & Cheng, L. (2017, January). Experimental analysis of high temperature PEEK materials on 3D printing test. In 2017 9th International conference on measuring technology and mechatronics automation (ICMTMA) (pp. 13-16). IEEE.

[38] Stoempie. (2017, August 21). Temp Tower PLA,ABS,PETG by stoempie. Retrieved from https://www.thingiverse.com/thing:2493504/files

[39] Levenhagen, N. P., & Dadmun, M. D. (2018). Interlayer diffusion of surface segregating additives to improve the isotropy of fused deposition modeling products. Polymer, 152, 35-41.

[40] Galati, M., & Minetola, P. (2020). On the measure of the aesthetic quality of 3D printed plastic parts. International Journal on Interactive Design and Manufacturing (IJIDeM), 14(2), 381-392.

[41] Turner, B. N., & Gold, S. A. (2015). A review of melt extrusion additive manufacturing processes: II. Materials, dimensional accuracy, and surface roughness. Rapid Prototyping Journal.

[42] Alberts, S. (2017, October 02). Basic Retraction test. Retrieved from https://www.thingiverse.com/thing:2563909

[43] IDig3Dprinting. (2016, January 19). XYZ 20mm Calibration Cube. Retrieved from https://www.thingiverse.com/thing:1278865

[44] Jiang, J., Stringer, J., Xu, X., & Zhong, R. Y. (2018). Investigation of printable threshold overhang angle in extrusion-based additive manufacturing for reducing support waste. International Journal of Computer Integrated Manufacturing, 31(10), 961-969.

[45] Majada107. (2018, February 25). *MINI* All In One 3D printer test. Retrieved from https://www.thingiverse.com/thing:2806295

[46] Prabhakar, M. M., Saravanan, A. K., Lenin, A. H., Mayandi, K., & Ramalingam, P. S. (2021). A short review on 3D printing methods, process parameters and materials. Materials Today: Proceedings, 45, 6108-6114.

[47] ASTM Standard F37-06 (2019), "Standard Test Methods for Sealability of Gasket Materials", ASTM International, West Conshohocken, PA, 2006, DOI: 10.1520/F0037-06R19, www.astm.org

[48] ASTM Standard F38 - 18 (2018), "Standard Test Methods for Creep Relaxation of a Gasket Material", ASTM International, West Conshohocken, PA, 1995, DOI: 10.1520/F0038-18, www.astm.org

[49] Chien, C. H., Hu, Y. L., Su, T. H., Liu, H. T., Wang, C. T., Yang, P. F., & Lu, Y. X. (2016). Effects of bolt pre-loading variations on performance of GDL in a bolted PEMFC by 3-D FEM analysis. Energy, 113, 1174-1187.

[50] Liu, W., Qiu, D., Peng, L., Yi, P., & Lai, X. (2020). Mechanical degradation of proton exchange membrane during assembly and running processes in proton exchange membrane fuel cells with metallic bipolar plates. International Journal of Energy Research, 44(11), 8622-8634.

[51] Nagaraj, S. K., Shivanna, S., Subramani, N. K., & Siddaramaiah, H. (2016). Revisiting powder X-ray diffraction technique: A powerful tool to characterize polymers and their composite films. J. Mater. Sci, 4, 1-5.

[52] Murthy, N. S., & Minor, H. (1995). Analysis of poorly crystallized polymers using resolution enhanced X-ray diffraction scans. Polymer, 36(13), 2499-2504.

[53] Gohn, A. M., Rhoades, A. M., Wonderling, N., Tighe, T., & Androsch, R. (2017). The effect of supercooling of the melt on the semicrystalline morphology of PA 66. Thermochimica Acta, 655, 313-318.

8   CURRICULUM VITA

Robert Anthony Lazarin attended the University of Texas at El Paso in the summer of 2017 to play football and obtain a degree in Mechanical Engineering. He began his research experience at UTEP under the direction of Dr. Calvin M. Stewart in his research group "Materials at Extremes Research Group", or MERG, in April of 2020. On December 12, 2020, Robert graduated with his Bachelor of Science in Mechanical Engineering degree. Wanting to further his education and continue his research, Robert applied and was accepted to the Master of Mechanical Engineering program. During this time, Robert continued his research of material extruded gaskets for proton exchange membrane fuel cells. He completed two summer internships in the summers of 2021 and 2022 at Los Alamos National Laboratory with his mentor, Tommy Rockward, in the group MPA-11, Materials Synthesis and Integrated Devices.